Coastal Engineering 147 (2019) 138–148

Contents lists available at ScienceDirect

Coastal Engineering

journal homepage: www.elsevier.com/locate/coastaleng

# Wave damping by flexible vegetation: Connecting individual blade dynamics to the meadow scale

Jiarui Lei*, Heidi Nepf

*Department of Civil and Environmental Engineering, Massachusetts Institute of Technology, Cambridge, MA, United States*

ARTICLE INFO

*Keywords:*
Reconfiguration
Flexible vegetation
Effective blade length
Wave damping

ABSTRACT

Aquatic vegetation provides ecosystem services of great value, including the damping of waves, which protects shorelines and reduces resuspension. This study proposes a physically-based model to predict the wave decay associated with a submerged meadow as a function of plant morphology, flexibility, and shoot density. In particular, the study considers both the rigid (sheath) and flexible (blade) segments of the plant. Flexible plants reconfigure in response to wave orbital velocity, which diminishes wave decay relative to a rigid plant of the same morphology. The impact of reconfiguration on wave decay can be characterized using an effective blade length, $l_e$, which represents the length of a rigid blade that generates the same drag as the flexible blade of length $l$. The effective blade length depends on the Cauchy number, which defines the ratio of hydrodynamic drag to blade stiffness, and the ratio of blade length to wave orbital excursion. This laboratory study considered how the scaling laws determined for individual blades can be used to predict the wave decay over a meadow of multiple plants, each consisting of multiple blades attached at a rigid stem (sheath). First, the drag force on and motion of individual model blades (made of low-density polyethylene) was studied for a range of wave conditions to provide empirical coefficients for the theoretically determined scaling laws for effective blade length, $l_e$. Second, the effective blade length predicted for individual blades was incorporated into a meadow-scale model to predict wave decay over a meadow. The meadow-scale model accounts for both the rigid and flexible parts of individual plants. Finally, wave decay was measured over meadows of different plant density (shoots per bed area), and the measured decay was used to validate the wave-decay model. Wave decay was shown to be similar over meadows with regular and random arrangements of plants.

## 1. Introduction

Submerged aquatic vegetation (SAV) provides a variety of ecosystem services with an estimated annual value of more than four trillion dollars (Costanza et al., 1997). It supports biodiversity by providing different habitats and shelter areas for many fisheries (Costanza et al., 1997) and by supplying food for herbivorous animals such as the dugong and green turtle (Waycott et al., 2005). Vegetation attenuates incoming waves and protects shorelines from erosion due to wave impact (e.g. Barbier et al., 2011; Arkema et al., 2017). As a carbon sink, seagrasses sequester a larger amount of carbon per hectare per year than rainforests (Fourqurean et al., 2012). In shallow marine and freshwater environments, wave-driven resuspension is a key factor in nutrient and light levels, controlling water quality and creating a positive feedback between vegetation and light-climate (e.g. Gacia and Duarte, 2001; Moore et al., 2004; Gruber and Kemp, 2010; Wang et al., 2015). Because aquatic vegetation plays such an important role through these processes, its protection and restoration have become a major focus in coastal management (Greiner et al., 2013; Sutton-Grier et al., 2015).

Many researchers have described the wave dissipation by submerged vegetation using a fitted drag coefficient, $C_D$, to characterize the drag force that the vegetation imposes on the flow (e.g. Mendez and Losada, 2004; Startigaki et al., 2011; Houser et al., 2015). Previous studies have expressed $C_D$ as a function of the vegetation Reynolds number ($Re = U_w b/\nu$, with $U_w$ the orbital wave velocity, $b$ the plant width, and $\nu$ the kinematic viscosity) and/or the Keulegan-Carpenter number ($KC = U_w T/b$, with $T$ the wave period) (e.g. Mendez and Losada, 2004). These models have been developed from both laboratory (Houser et al., 2015; Stratigaki et al., 2011) and field studies (Bradley and Houser, 2009). Models using the orbital wave velocity in a quadratic drag law can work well for rigid vegetation, but flexible vegetation moves with the water so that the relative velocity between the water and the vegetation is not the wave velocity. For example, the tip

* Corresponding author.
*E-mail address:* garylei@mit.edu (J. Lei).

https://doi.org/10.1016/j.coastaleng.2019.01.008
Received 19 February 2018; Received in revised form 16 October 2018; Accepted 22 January 2019
Available online 19 February 2019
0378-3839/ Published by Elsevier B.V.

of a flexible seagrass blade can move passively with a wave whose wave excursion is comparable to or less than the blade length (Luhar and Nepf, 2016). Under these conditions, there is negligible relative velocity and thus negligible drag at the blade tip. Because the relative motion is diminished from the orbital wave velocity over part of the flexible blade length, the blade experiences less drag than a geometrically similar but rigid blade in the same wave conditions.

A number of studies have tried to account for relative motion in the drag formulation. For example, in the theoretical analysis of Mendez et al. (1999) the blade excursion was treated as a function linearly proportional to the distance along the blade, and the drag was calculated using the relative velocity. In the field study by Bradley and Houser (2009), blade tip excursion was recorded with a camera and used to estimate blade motion along the blade length. In the numerical study of Maza et al. (2013), the relative velocity was obtained by considering a linear deformation of the plant. In Zeller et al. (2014), a single blade was numerically modeled as a series of rigid elements linked together, and the blade motion was incorporated into the calculation of drag. Finally, in the laboratory study of Luhar and Nepf (2016), the blade motion was digitally recorded, and the observed blade velocity was used to calculate the relative velocity and drag.

The degree of plant flexibility plays an important role in determining the relative velocity. A few studies have modeled vegetation blades as flat plates (Mendez et al., 1999) or cantilever beams (e.g. Bradley and Houser, 2009; Mullarney and Henderson, 2010). These models work well for vegetation that undergoes mild deformation, e.g. displacements that are much less than the plant length. However, more flexible vegetation, such as seagrass, can experience significant deformation (Luhar and Nepf, 2016). The deformation in response to flow is known as reconfiguration, and the degree of reconfiguration is described by three dimensionless parameters, the wave Cauchy number $Ca_w$, which is the ratio of the hydrodynamic drag to the restoring force due to blade stiffness, the Buoyancy parameter $B$, which is the ratio between the restoring forces due to buoyancy and stiffness (Luhar and Nepf, 2011), and the blade length ratio $L$, which compares the blade length to the wave excursion (Luhar and Nepf, 2016),

$$Ca_w = \frac{\rho b U_w^2 l^3}{EI} \tag{1}$$

$$B = \frac{\Delta\rho g b t l^3}{EI} \tag{2}$$

$$L = \frac{l}{A_w} = \frac{2\pi l}{U_w T} \tag{3}$$

Here, $\rho$ is the density of water, $b$ is the blade width, $l$ is the blade length, $t$ is the blade thickness, $\Delta\rho$ is the difference in density between the water and the blade, $E$ is the Young's modulus, $I = \frac{bt^3}{12}$ is the second moment of inertia, and $A_w$ ($= U_w T/2\pi$) is the wave excursion (wave orbital radius). For common seagrass species, such as *Thalassia testudinum*, *Posidonia oceanica* and *Zostera marina,* $B$ is small because blades are close to neutrally buoyant, in which case $B$ does not provide an important control on blade motion (Luhar and Nepf, 2016).

To describe the impact of reconfiguration on the drag of an individual blade, Luhar and Nepf (2011, 2016) proposed the effective blade length, $l_e$, defined as the length of a rigid, vertical blade that generates the same drag as the flexible blade of length $l$. The ratio $l_e/l$ is a function of $Ca_w$ and $L$. For a small wave excursion, $L \gg 1$ or $A_w \ll l$, the blade bending-angle ($\theta$) can be approximated as the ratio of blade tip excursion to blade length. Further, the blade tip excursion scales on the wave excursion, so that $\theta \sim A_w/l$. Balancing the drag force and the elastic restoring force of the blade implies $(A_w/l_e^3) \sim \rho b l_e U_w^2$, from which

$$\frac{l_e}{l} \sim (Ca_w L)^{-1/4} \tag{4}$$

Luhar and Nepf (2016) validated this scaling for individual blades with $L$ as small as 1.5. The same scaling was also verified for individual blades within a meadow (Luhar et al., 2017). The present study uses this scaling law to construct a predictive model for wave decay over a meadow.

### 1.1. Wave decay over a meadow of submerged plants

Dalrymple et al. (1984) described wave decay over a meadow of submerged plants (see also Mendez and Losada, 2004; Bradley and Houser, 2009). Assuming linear wave theory and that energy dissipation is caused only by the meadow, the steady wave energy balance is

$$-E_v = \frac{\partial}{\partial x}\left(\frac{1}{2}\rho g a_w^2 c_g\right) \tag{5}$$

in which $E_v$ is the rate of wave energy dissipation due to the vegetation, $g$ is acceleration due to gravity, $a_w$ is wave amplitude, and $c_g$ is wave group velocity. Assuming rigid, vertical blades of length $l$ and using a quadratic drag law, the rate of energy dissipation by the vegetation can be expressed as

$$E_v = \frac{1}{T}\int_{t=0}^{T}\int_{z=0}^{l}\frac{1}{2}C_D a_v |u_R| u_R u \, dz \, dt \tag{6}$$

The parameter $a_v$ is the vegetation frontal area per unit meadow volume, which is defined as $a_v = n_v b$, with blade width, $b$, and blades per bed area, $n_v$. $u_R$ is the relative velocity between the vegetation and the water, and $u$ is the absolute water velocity. The vertical coordinate, $z$, is zero at the bed and positive upward. Given the slender morphology of a seagrass blade, the vertical drag force has been assumed to be negligible compared to the horizontal drag force.

For rigid vegetation, the relative velocity between the vegetation and the water is the absolute fluid velocity, $u_R = u$. Assuming linear waves, the horizontal velocity within the meadow is

$$u = \alpha \, a_w \, \omega \frac{\cosh(kz)}{\sinh(kh)}\sin(\omega t) \tag{7}$$

in which $\omega = 2\pi/T$ is the radian frequency, $k = 2\pi/\lambda$ is the wave number for wavelength $\lambda$, and $h$ is the water depth. Note that (7) includes the reduction in orbital velocity due to drag and inertial forces exerted by the canopy elements, which is represented by factor $\alpha$ (= ratio of in-canopy velocity to free-stream velocity), as defined in Lowe et al. (2005). Assuming $C_D$ and $a_v$ are constant, equations (5)–(7) can be combined to yield

$$\frac{\partial}{\partial x}\left(\frac{1}{2}\rho g a_w^2 c_g\right) = \frac{2}{3\pi}\rho C_D a_v \left(\frac{\alpha a_w \omega}{\sinh(kh)}\right)^3 \left(\frac{9\sinh(kl) + \sinh(3kl)}{12\,k}\right) \tag{8}$$

which has a solution of the form

$$\frac{a_w(x)}{a_{w0}} = \frac{1}{1 + K_D \, a_{w0} \, x} \tag{9}$$

Here, $a_{wo}$ is the wave amplitude at the beginning of the meadow, $x = 0$ cm, and $K_D$ is the wave decay coefficient, defined as

$$K_D = \frac{2}{9\pi} C_D a_v k \, \alpha^3 \left(\frac{9\sinh(kl) + \sinh(3kl)}{\sinh kh\,(\sinh(2\mathrm{kh}) + 2kh)}\right) \tag{10}$$

Equation (10) assumes rigid vegetation and adjustments are needed for application to flexible vegetation. In particular, for $Ca_w > 1$, the blade moves in response to the wave, so that the assumption $u_R = u$ is no longer reasonable. As noted above, several studies have incorporated the impact of blade motion into a fitted drag coefficient (e.g. Mendez and Losada, 2004; Stratigaki et al., 2011; Manca et al., 2012; Maza et al., 2013; Houser et al., 2015). Losada et al. (2016) observed wave damping by flexible vegetation in both pure waves and combined wave-current flows, and they improved the description of wave damping by replacing the blade length in eqn. (10) with the measured deflected plant height. Similarly, Luhar et al. (2017) suggested the use of a

constant drag coefficient, assigned based on the rigid plant geometry, and incorporated the impact of blade motion through an effective length, $l_e$. Following this framework, eqn. (10) can be adjusted by replacing $l$ with $l_e$. In Luhar et al. (2017), $l_e$ was inferred from observed blade motion, and the resulting estimates of $K_D$ agreed with measured values to within 20% for most cases. The present study advances the concept of effective blade length by considering whether a scaling law for individual blades can be used to predict the blade effective length used in the prediction of $K_D$, eliminating the need for blade motion observations, as used in Losada et al. (2016) and Luhar et al. (2017). First, the drag force on and motion of individual blades were studied for a range of wave conditions to provide the empirical coefficient in the blade scaling law (eqn. (4)). Second, a model was constructed to predict wave decay over a meadow of plants consisting of multiple blades attached at a rigid stem, representing the sheath. Third, the wave decay was measured over meadows of different meadow density (stems per bed area) and used to validate the model.

## 2. Materials and methods

The laboratory experiments were conducted in a 24-m long water channel with a width of 38 cm. For experiments on individual blades, the water depth was $h = 40$ cm. For experiments with a model meadow, the water depth was varied between $h = 18$ cm and 45 cm. Monochromatic waves were generated with a piston-type wave maker. Wave reflection was reduced using a beach with a 1:5 slope that was covered with 9 cm of rubberized coconut fiber. Following the method from Goda and Suzuki (1977), the wave reflection was measured using two simultaneous wave gages. The assessment of reflection was made at mid-channel, where the meadow was positioned, but without the meadow. Across multiple wave conditions the measured wave reflection was 7 ± 3%.

### 2.1. Model seagrass blades and meadow

Experiments were conducted using both individual blades and meadows of different shoot density. Individual blades were constructed from LDPE (low-density polyethylene) film, with a material density of 0.925 g/cm$^3$ and a Young's modulus of 0.3 GPa (Ghisalberti and Nepf, 2002). To cover a wide range of $Ca_w$ and $L$, four different blade lengths (3 cm, 5 cm, 10 cm and 15 cm) and two blade thicknesses (100 μm and 250 μm) were considered. The meadow of model seagrass was constructed with individual plants consisting of six LDPE blades and a cylindrical wooden stem. The stems were inserted into a plastic baseboard in a staggered array of holes (Fig. 1). Once inserted, the stem extended 1 cm above the bed. The blades were cut 14 cm long, $b = 3$ mm wide, and $t = 100$ μm thick. Six blades were attached to each stem with 1-cm overlap using a 1-cm wide strip of waterproof tape that covered the entire expose cylinder. The end of the blades attached to the rigid stem mimicked the sheath of real seagrasses. The diameter of the stem with attached blades (sheath) was measured with micrometer to have a diameter of $d = 0.69 \pm 0.02$ cm. Because the stem and blades had 1-cm overlap, the fully erect plant was $l_p = 14$ cm tall. The model meadow extended over the full channel width and 3.5–7 m along the channel. Plant densities 280, 600, 850, 1050, and 1370 plants/m$^2$ were considered. The stem configuration for three of the meadow densities is shown in Fig. 1(a) (b) (c).

For both the individual blades and the meadow, wave amplitude, $a_w$, was varied between 0.8 and 5 cm. Three wave periods were considered: $T = 2.0$, 1.4 and 1.0 s. During individual blade drag measurements, velocity was measured 6.5 cm above the bed using a Nortek Vectrino at a sampling rate of 200 Hz for 3 min. During wave damping measurements, velocity was measured at the top of the meadow at a sampling rate of 200 Hz for 3 min. For most wave conditions $k \times l < 0.32$, for which linear wave theory indicates that the difference in velocity over the height of the blade was less than 5%, indicating that a velocity record at a single vertical position was sufficient. With 200 samples per second, the velocity record could be binned into $\gamma = 200 \times T$ phase bins per wave to find the phase-averaged velocity $\widetilde{u_w}(\phi)$. The phase-average velocity in the $n^{th}$ phase bin ($n = 1$ to $\gamma$), which has phase $\phi = 2\pi n/\gamma$ is

$$\widetilde{u_w}(\phi(n)) = \widetilde{u_w}\left(\frac{2\pi n}{\gamma}\right) = \frac{1}{N}\sum_{m=0}^{N-1} u_w(n+\gamma m) \tag{11}$$

in which $\widetilde{u_w}$ denotes the phase-averaged velocity, $N$ is the number of wave periods in the record, and $u_w(n+\gamma m)$ is the $(n+\gamma m)^{\text{th}}$ velocity sample. The orbital wave velocity $U_w$ was calculated as $\sqrt{2}$ times the rms of the phase-averaged velocity, and it varied from 4 cm/s to 20 cm/s, such that the experimental conditions included $Ca_w$ from 0.1 to 5000, and $L$ from 0.5 to 12.4 for individual blades. For the meadow cases, $Ca_w$ ranged from 90 to 3800, and $L$ ranged from 2 to 26. These values of $Ca_w$ and $L$ overlap with a wide range of field conditions with wind waves ($T = 1$ to 2 s), as shown in Table 1.

The movement of individual blades in isolation and individual blades within the meadow was recorded with a Canon 5D Mark III DSLR camera (serial No. 358023001794). Video was recorded at 50 frames per second for 1 min, and the video was processed using the image processing toolbox in MATLAB (version R2014b). Individual blades were marked with four black dots at 4, 7, 10 and 13 cm along the blade, which were tracked through digital processing.

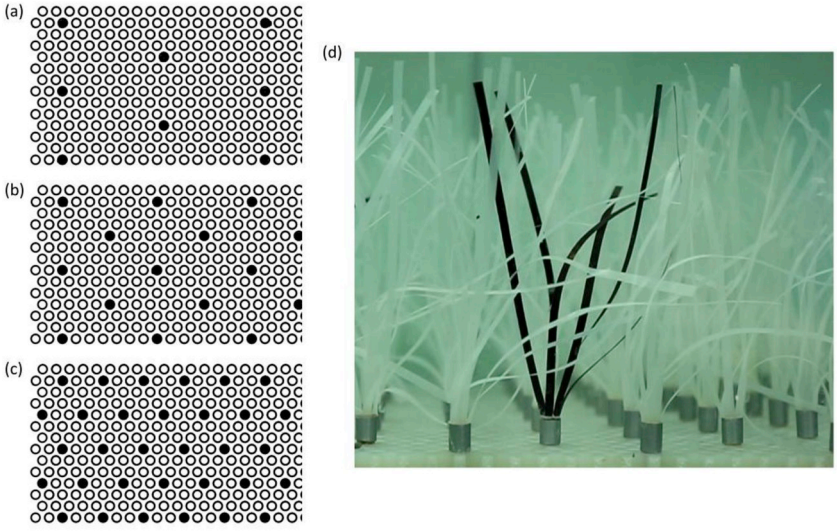


**Fig. 1.** Section of baseboard showing staggered holes (circles) and stem pattern (filled circles) at stem density (a) 280, (b) 600, and (c) 1370 plants/m$^2$. Adjacent holes were 0.95 cm apart measured center to center. (d) Model seagrass meadow with 600 plants/m$^2$. To help visualize an individual plant within the meadow, one plant was colored black. Image taken without waves, so blades are stationary. For digital video processing, individual blades were marked with just four dots at 4, 7, 10 and 13 cm along the blade.

**Table 1**
Physical parameters of real seagrass blades.

| Physical parameters | *Thalassia testudinum*[a] | *Zostera marina*[b] | *Posidonia oceanica*[c] | Experiments w/single blade | Experiments w/meadow |
|---|---|---|---|---|---|
| Thickness, $t$(mm) | 0.30 to 0.37 | 0.15 to 0.23 | 0.20 | 0.10, 0.25 | 0.10 |
| Width, $b$(mm) | 10 | 3 to 5 | 10 | 10 | 3 |
| Length, $l$(cm) | 10 to 25 | 15 to 60 | 15 to 50 | 3, 5, 10, 15 | 13 |
| Density, ρ (kg/m$^3$) | 940 | 700 | 910 | 925 | 925 |
| Modulus, $E$ (GPa) | 0.4 to 2.4 | 0.3 | 0.5 | 0.3 | 0.3 |
| $Ca_w$ (eqn. (1)) | 0.16 to 640 | 16 to 80000 | 16 to 14000 | 0.1 to 5300 | 87 to 3800 |
| $L$ (eqn. (3)) | 0.5 to 2.5 | 0.7 to 6.0 | 0.7 to 5.0 | 0.5 to 12.4 | 2.0 to 26.0 |
| Wave velocity $U_w$ (m/s) | 0.3 to 1.3 | 0.3 to 1.3 | 0.3 to 1.3 | 0.04 to 0.2 | 0.04 to 0.2 |
| Frontal area/bed area, $a_v l$ | 3 to 7 | 0.3 to 2 | 11 to 15 | | 2 to 8 |

[a] Bradley and Houser, (2009), Weitzman et al., (2013).
[b] Fonseca et al., (2007), Abdelrhman (2007), Moore (2004), McKone (2009).
[c] Folkard (2005), Infantes et al., (2012).

### 2.2. Drag measurements on individual blades

Drag measurements were made on individual blades without a meadow. A single blade was inserted into a 4-cm tall stainless steel post (2 mm diameter) attached to a submersible force transducer (Futek LSB210). The accuracy of the force transducer was 10%, and the resolution was 0.001 N. The force transducer was mounted in a 12-cm high acrylic ramp that spanned the channel width. The ramp was 1-m long on the top and 2-m at the bed (Fig. 2). For each wave condition, the drag force on the blade and post ($F_t(t)$) was measured for 3 min at a sampling rate of 2000 Hz. A separate experiment was conducted to measure the force on the post alone ($F_p(t)$), i.e. without blade, for the same wave conditions. With 2000 samples per second, and for a wave period of $T$ [sec], there will be (2000 x $T$) samples per wave, which were each assigned to a different phase bin, such that there are ($\gamma$ = 2000 x $T$) phase bins within each wave. Because the force record was 3-min long, which included ninety 2-s waves, each phase-bin has ninety samples from which the phase average was calculated. The phase-average force in the $n^{th}$ phase bin ($n$ = 1 to $\gamma$), which has phase $\phi = 2\pi n/\gamma$ was then determined as

$$\tilde{F}(\phi(n)) = \frac{1}{N}\sum_{m=0}^{N-1} F(n+\gamma m) \tag{12}$$

in which $N$ is the number of wave periods in the record, and $F(n+\gamma m)$ is the $(n+\gamma m)^{th}$ force sample. The maximum force on the blade within one wave cycle, $F_{b,max}$, was estimated as the maximum phase-averaged force on the blade and post together ($F_{t,max}$) minus that maximum phase-averaged force on the post alone ($F_{p,max}$). Specifically, $F_{b,max} = F_{t,max} - F_{p,max}$.

The measured effective length ratio, $l_e/l$, was defined as the ratio of measured maximum force to the expected maximum force for a rigid blade of the same geometry.

$$\frac{l_e}{l} = \frac{\textit{measured maximum force}}{\textit{expected maximum force for rigid blade}} = \frac{F_{b,max}}{F_{rigid,max}} \tag{13}$$

The time-varying force on a rigid blade can be described as

$$F(t) = \int_0^l \frac{1}{2}\rho C_D b|u_w|u_w + \rho\left(\frac{1}{4}b^2C_M + bd\right)\frac{\partial u_w}{\partial t}dz \tag{14}$$

The first term inside the integral is the drag, and the second term is the added mass and buoyancy. The drag ($C_D$) and added mass ($C_M$) coefficients depend on the Keulegan-Carpenter number ($KC$), as described in Sarpkaya and O'Keefe (1996). Eqn. (14) has been validated using the measured time-dependent force on an individual blade, as described in Luhar and Nepf (2016). Since the maximum force occurs at the maximum velocity, at which time the added mass term is negligible, the maximum force on a rigid blade is simply,

$$F_{rigid,max} = \int_0^l \frac{1}{2}\rho C_D b|\tilde{u}_{w,max}|\tilde{u}_{w,max}dz \tag{15}$$

with $\tilde{u}_{w,max}$ the measured, maximum, phase-averaged velocity. The drag coefficient, $C_D$, was estimated from $KC$ and Fig. 13 in Keulegan and Carpenter (1958). The range of $KC$ was 8 to 40, yielding $C_D$ from 3.1 to 5.3.

### 2.3. Measured wave decay coefficient $K_D$

The decay of wave amplitude over a meadow was measured using two wave gages (Fig. 3). A reference wave gage was permanently mounted upstream of the meadow ($x$ = −125 cm). The variation in wave amplitude at this gage over the duration of each experiment (≈80 min) was less 3%, confirming stationary wave conditions. A second wave gage was mounted on a trolley that moved along the flume on precision rails. The moving gage collected data at 10 or 20 cm intervals (depending on the wave length) starting 40 cm upstream of the meadow and continuing along the entire length of the meadow. At each $x$ position, the instantaneous position of the water surface, $\eta$(t), was measured at 1 kHz for 1 min (30 to 60 waves, depending on wave period). The variation in the waveform was negligible (less than 2%) over this time (1 min). The wave amplitude $a_w$ was calculated from the

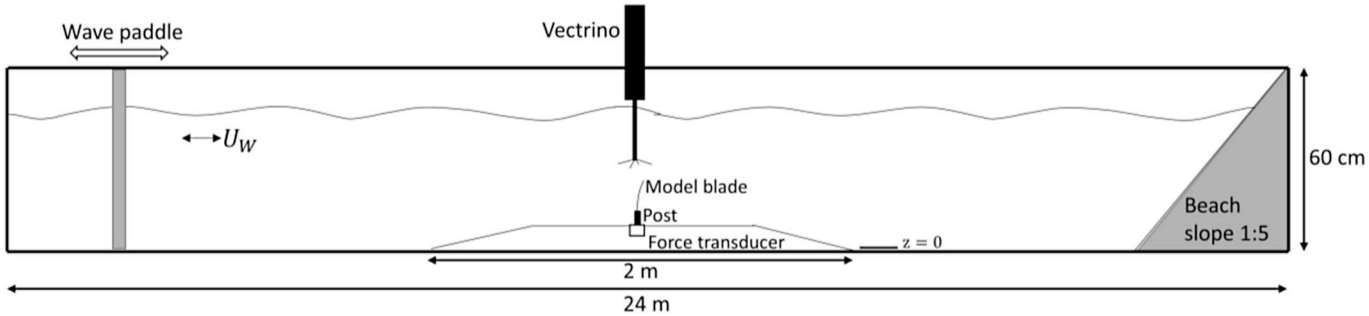


**Fig. 2.** Experimental setup for measuring force on a single blade. Mean water depth $h$ = 40 cm. Figure is not to scale. The velocity measurement was taken without the model blade with the Vectrino placed directly above the blade post.

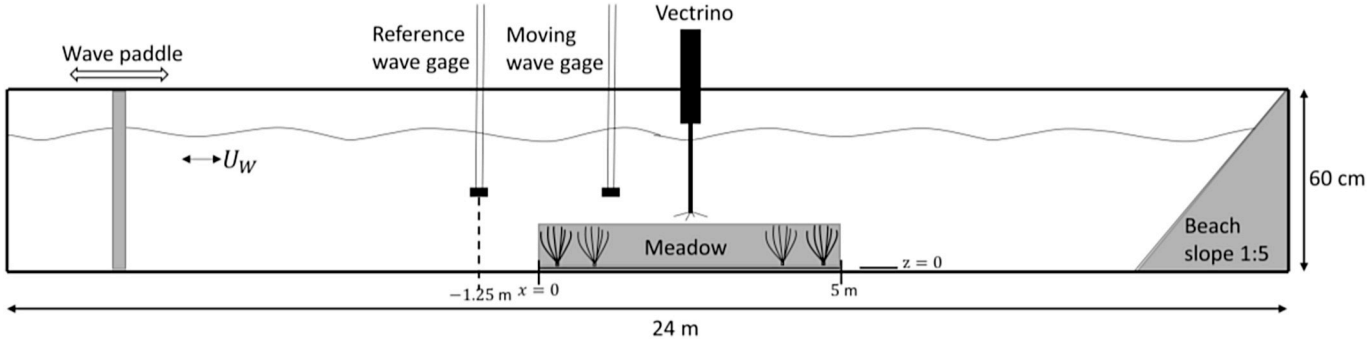


**Fig. 3.** Experimental setup for wave damping measurements (not to scale). The Vectrino was placed at mid-meadow length and measured the velocity at the top of the meadow.

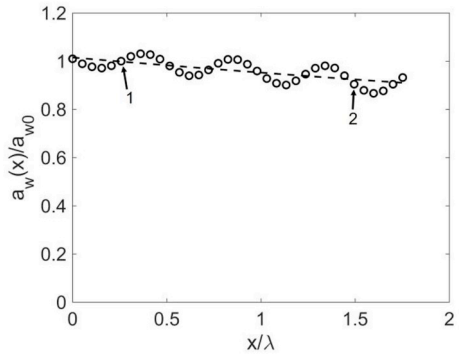


**Fig. 4.** Wave amplitude evolution, $\frac{a_w(x)}{a_{w0}}$ versus $\frac{x}{\lambda}$, for a wave with amplitude $a_{w0} = 2.96 \pm 0.04$ cm, period $T = 2$ s, and wavelength $\lambda = 3.7$ m. The stem density was 600 stems $m^{-2}$. The dashed line indicates the best fit of eqn. (9) between point 1 and 2, which are located at nodes in the wave beat pattern. The beat pattern results from the constructive interference of the wavemaker wave train with its reflection off the beach.

root-mean-square surface displacement, $a_w = \sqrt{\frac{2}{T}\int_0^T \eta^2(t)dt}$. The wave decay coefficient, $K_D$, was found by fitting eq. (9), an example of which is shown in Fig. 4. Due to wave reflection, the amplitude contained beats at intervals of ½ $\lambda$. A new fitting method was developed to minimize the influence of these beats on the fit (see supplementary material). In the example shown (Fig. 4), the fit was applied to all measured data between the points marked 1 and 2. Point 1 was selected as the closest to the first node of the beat pattern. Point 2 was 2.5$\lambda$ from point 1, which satisfied the requirement to span a phase difference of $\left(n + \frac{1}{2}\right)\pi$, with integer $n$ (see supplementary material). Uncertainty was introduced from the choice of fit points, which was assessed by considering different start and end points adjacent to the nodes. In the case shown, $a_{wo} = 2.96 \pm 0.04$ cm and the fitted $K_D a_{w0}\lambda = 0.061 \pm 0.004$. Because wave energy can also be reduced by viscous boundary layers on the sidewalls and flume bed, the experiment was repeated without the meadow for each wave period. The viscous damping does not depend on wave amplitude (Hunt, 1964). For the bare channel $K_D a_{w0}\lambda = 0.010 \pm 0.001$ across all wave periods. This bare-channel decay was subtracted from each meadow condition to isolate the wave damping due only to the meadow. The uncertainty in the fitted $K_D a_{w0}\lambda$ and fitted $a_{wo}$ was propagated to find the uncertainty in fitted $K_D$. For the case shown in Fig. 4, $K_D = (0.67 \pm 0.05)m^{-2}$.

## 3. Results

### 3.1. Individual blades and effective blade length

For individual blades in waves, the measured effective blade length followed the scaling law $l_e/l \sim (Ca_w L)^{-1/4}$ across several decades of $Ca_w L$ (Fig. 5). The blade dimensions and wave conditions are summarized in Table S1 in the supplementary material. The lower panel of Fig. 5 shows images extracted from digital videos of individual blades under 2-s waves. Each image represents a stack of 20 black and white images with time step = 0.1 s (5 frames). The same image processing was performed at different times along the total video, from which the variability in horizontal blade tip excursion was shown to by less than 20%.

For $1 < Ca_w L < 10{,}000$ the fitted line with 95% C.I. was

$$\frac{l_e}{l} = (0.94 \pm 0.06)(Ca_w L)^{-0.25\pm0.02} \tag{17}$$

For $Ca_w L < 1$, $l_e/l$ was equal to 1 within uncertainty, indicating that the flexible model blade behaved like a rigid blade, $l_e = l$ (blade image 1 in Fig. 5). Note that when $Ca_w$ is close to 1, measured $l_e$ can be greater than $l$, indicating that the force was enhanced relative to a rigid blade. As shown in previous studies, when $Ca_w$ is close to 1, the vegetation motion is 90° out of phase with the water motion, and this phase deference generates higher relative velocity between vegetation and water than occurs for a completely rigid blade, which then yields a greater measured force than for a completely rigid blade, i.e. $l_e/l > 1$ (Mullarney and Hendersen, 2010; Luhar et al., 2016). As $Ca_w L$ increased there was a shift in blade motion from cantilever-like motion (blade images 2 and 3) to higher modes of motion (blade images 4 and 5). A similar transition in plant motion with decreasing non-dimensional stiffness (analogous to increasing $Ca_w L$) was noted in Mullarney and Henderson (2010). Note that for cases 3 to 5 the horizontal excursion of the blade tip through the wave cycle was comparable to the wave orbital diameter ($2A_w$, shown with horizontal blue line in Fig. 5). In addition, for cases 4 and 5 the blade motion was asymmetric. This asymmetry arose from the contribution of the vertical velocity component. Specifically, the progression of linear wave orbital velocity acting on the blade (*i.e.* forward velocity, downward velocity, backward velocity, upward velocity) produces asymmetric blade motion (see Fig. 5.6 in Dobkin, 2015; Gijon Mancheno, 2016). The effective length describes the length of blade over which there is significant relative motion between the blade and the water, and only this region of the blade ($z < l_e$) contributes significantly to drag. The upper part of the blade ($z > l_e$) moves nearly passively with the water, imparting very little drag. This behavior is also noted in Mullarney and Henderson (2010), who used an analytical model of flexible, single-stemmed vegetation to show that wave energy dissipation is concentrated in a near-bed layer within which the motion of the plant reduces smoothly to zero. This region is called the elastic boundary layer, because it defines the length of stem over which elastic bending forces contributed significantly to stem deformation. The height of the elastic boundary layer scales with $(Ca_w L)^{-1/4}$, consistent with eqn. (17).

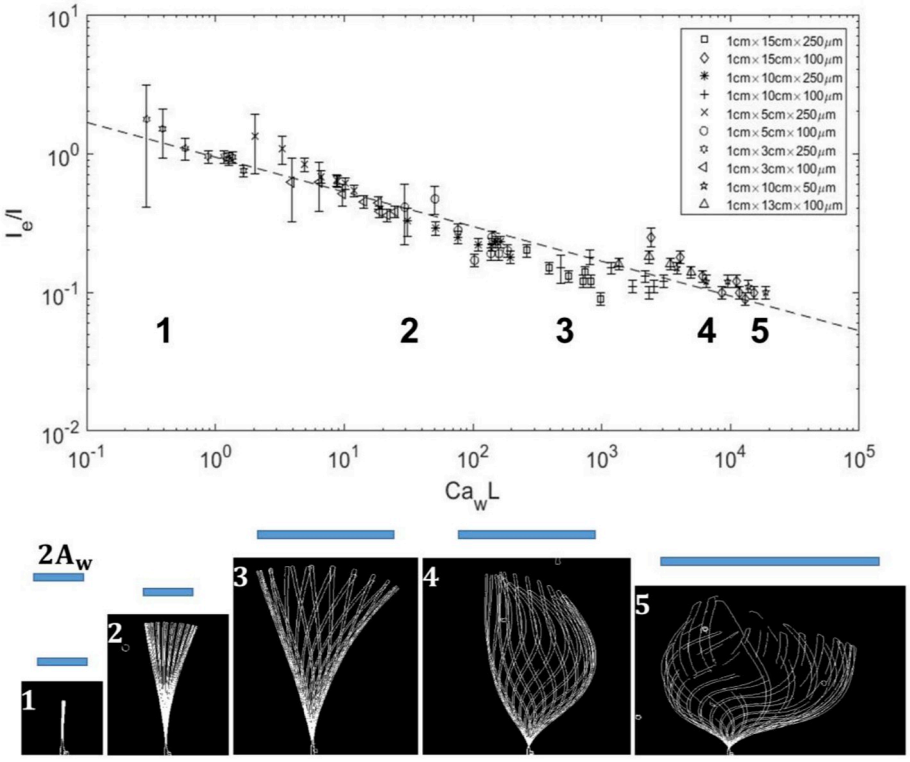


**Fig. 5.** Effective blade length, $l_e$, normalized by total blade length, $l$, as a function of wave Cauchy number, $Ca_w$, and non-dimensional wave excursion, $L$. The dashed line indicates the fitted equation, $l_e/l = (0.94 \pm 0.06)(Ca_w L)^{-(0.25\pm0.02)}$, with 95%CI. Bold numbers correspond to images at the bottom of figure, which show blade position through a wave cycle. Each image represents a stack of 20 black and white images, with time step = 0.1 s (5 frames). For all images the wave period was 2 s. The blue horizontal bars denote the wave orbital diameter ($2A_w$). Image 1: $Ca_w = 0.1$, $L = 2.5$; image 2: $Ca_w = 3.8$, $L = 8.3$; image 3: $Ca_w = 80$, $L = 5.0$; image 4: $Ca_w = 1250$, $L = 5.0$ ; image 5: $Ca_w = 4800$, $L = 2.5$. (For interpretation of the references to color in this figure legend, the reader is referred to the Web version of this article.)

### 3.2. Prediction of wave decay coefficient ($K_D$) using blade reconfiguration scaling-laws

Building on the scaling law for individual blades (section 3.1), a prediction of the wave decay coefficient, $K_D$, for a meadow was developed. Specifically, an effective meadow length-scale, $l_{e,m}$, was defined to account for plant morphology and blade reconfiguration. Replacing the total plant height ($l$) in eqn. (10) by the effective meadow height ($l_{e,m}$), the wave decay coefficient, $K_D$, can be predicted as

$$K_D = \frac{2}{9\pi} C_D a_v k \alpha^3 \left( \frac{9\sinh(kl_{e,m}) + \sinh(3\,kl_{e,m})}{\sinh kh(\sinh(2kh) + 2kh)} \right) \quad (18)$$

Losada et al. (2016) proposed a similar adaptation to eqn. (10), replacing the full blade length, $l$, with the measured mean deflected height. The current project advances this concept by providing a method to predict the effective meadow height without requiring an *a priori* measurement of blade posture. As shown in Figs. 1 and 6, individual model plants were constructed from six blades taped around a 1-cm tall rigid stem. This construction was intended to mimic the sheath of a real seagrass. Digital imaging revealed that blade motion was restricted near the sheath, due to the bundling of the blades within the sheath. To account for this, a section of the blade was assumed to be rigid. The length of the rigid segment, $l_r$, was estimated from digital images. Specifically, for each black blade, the rigid length was estimated as the distance above the bed within which that blade remained within the vertical region defined by the stem width (marked with grey shading in Fig. 6) through the wave cycle. This value was estimated for each of the six black blades within each of four different meadow densities (600, 830, 1050, 1370 stems $m^{-2}$), and for two wave conditions representing the high range of blade motion ($T$ = 1.4 and 2 s, $a_w$ = 3.5 cm and 3.9 cm, respectively). Using these 48 measurements, $l_r$= 2.3 ± 0.5 cm. To illustrate the range of blade motion, Fig. 6 (b) and (d) show blades at their maximum forward excursion, and Fig. 6 (a) and (c) show blades at the maximum backward excursion. Note that the rigid length differed between the six blades, based on their position around the sheath.

Recognizing that the individual plants consist of both rigid and freely moving (flexible) segments, the total shoot height ($l_s$, 14 cm) was broken into a rigid ($l_r$) and flexible segment. The flexible segment was assumed to behave like an isolated blade of length $l_b = l_s - l_r$, and its effective length ($l_{b,e}$) was determined from eqn. (17), using the flexible blade length, $l_b$, to define $Ca_w L$, denoted as $(Ca_w L)_b$. The effective meadow height was then defined as the sum of the rigid segment and the effective length of the flexible segment

$$l_{e,\,m} = 0.94(Ca_w L)_b^{-0.25} l_b + l_r \quad (19)$$

effective length flexible segment rigid segment

The wave decay coefficient, $K_D$, was predicted by combining eqns. (18) and (19). The predicted $K_D$ were compared to measured $K_D$ for different meadow and wave conditions, which are summarized in Table S2 in the supplementary information. Within eqn. (18), the drag coefficient $C_D$ was determined based on measurements on a rigid blade under the same wave conditions, $C_D = \max(10KC^{-1/3}, 1.95)$, as described in Luhar and Nepf (2016), based on Keulegan and Carpenter (1958). The reduction of in-canopy wave velocity relative to linear theory, $\alpha$ in eqn. (18), was computed using the numerical model described in Lowe et al. (2005). For the meadows considered here, $\alpha$ ranged from 0.84 to 0.98 (see Table S2 in supporting information). As a simpler alternative, eqn. (24) in Lowe et al. (2005) gives $\alpha_i = \frac{1-\lambda_p}{1+(C_M-1)\lambda_p}$, with $\lambda_p$ describing the solid volume fraction of the meadow. This simplification is reasonable when the wave excursion is comparable to or smaller than the stem spacing.

Fig. 7 compares the predicted and measured wave decay coefficients

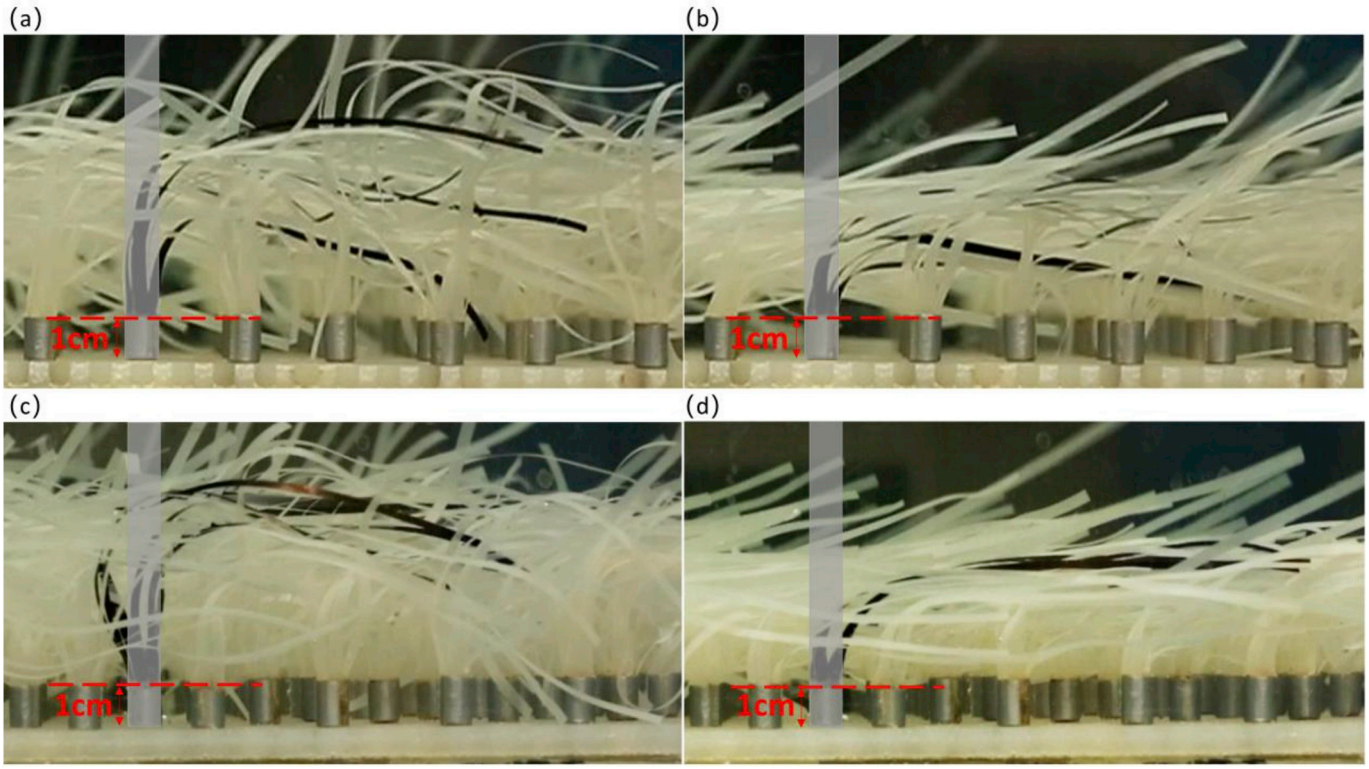


**Fig. 6.** Examples of the blade images used to define the section of blade near the sheath with restricted motion, $l_r$. (a) (b) Stem density $n = 850$ /m$^2$, wave period $T = 1.4$ s, and wave amplitude $a_w = 3.5$ cm, $Ca_w = 6.0 \times 10^3$; (c) (d) Stem density $n = 1370$ /m$^2$, wave period $T = 2$ s and wave amplitude $a_w = 3.9$ cm, $Ca_w = 5.6 \times 10^3$. In (b) and (d) blades are at their maximum forward excursion; in (a) and (c), blades are at their maximum backward excursion. The light grey shading is the vertical projection of the rigid stem. The vertical extent over which the blades were restricted to this grey zone throughout the wave cycle defined $l_r$, the rigid blade length. For reference, 1-cm distance is marked with red dashed line. (For interpretation of the references to color in this figure legend, the reader is referred to the Web version of this article.)

in linear and log scales. In the majority of cases, the predicted $K_D$ agreed with the measured $K_D$ within uncertainty. For the six data points on the upper right, $K_D$ was overpredicted by 44%. These cases corresponded to the highest wave decay, and the over-prediction may be attributed to the fact that the predicted $K_D$ was based on $Ca_wL$ measured at mid-length along the meadow, which would underestimate $Ca_wL$ at the start of the meadow (the reference point for decay) and therefore overestimate $K_D$ (because $K_D$ increases with decreasing $Ca_wL$, eqns. (18) and (19)). In the Discussion section, a method that accounts for the spatial evolution of $Ca_wL$ is suggested. A linear-fit of $K_D(predicted)$ versus $K_D(measured)$ had a slope of 1.40 ± 0.08 (95% CI).

Note that, as a simplification the rigid segment, $l_r$= 2.3 ± 0.5 cm, was assumed to represent both the circular stem and the constrained portion of blades. This simplification did not consider that the drag coefficient and frontal area of the circular stem was different from the six attached blades, i.e. $C_Da_v$ in eqn. (18) is different for the circular stem and the six blades. Specifically, the width, $d$ = 6.9 mm, and drag coefficient ($C_{D,stem}$ = 1.8 ± 0.2, based Keulegan and Carpenter, 1958) of the stem were different from the blades. To account for this, the stem length was adjusted to represent an equivalent $C_Da_v$ for 6 blades. This was called the effective stem-length, $l_{stem,e}$, defined by $C_{D,stem}l_{stem}d = C_D6bl_{stem,e}$, from which $l_{stem,e}$ = 0.3 cm. Making this adjustment, $l_r$ was reduced to 1.6 ± 0.5 cm. Using this in eqn. (19) improves the agreement between predicted and measured $K_D$ to $K_D(predicted) = (1.16 \pm 0.07)K_D(measured)$. Finally, it is important to note that the rigid ($l_r$) and effective blade lengths ($l_{b,e}$) made comparable contributions to effective meadow height, $l_{e,m} = l_{b,e} + l_r$, with $l_r/l_{b,e}$ = 1.01 ± 0.13. If the rigid segment was neglected, $l_r$ = 0,

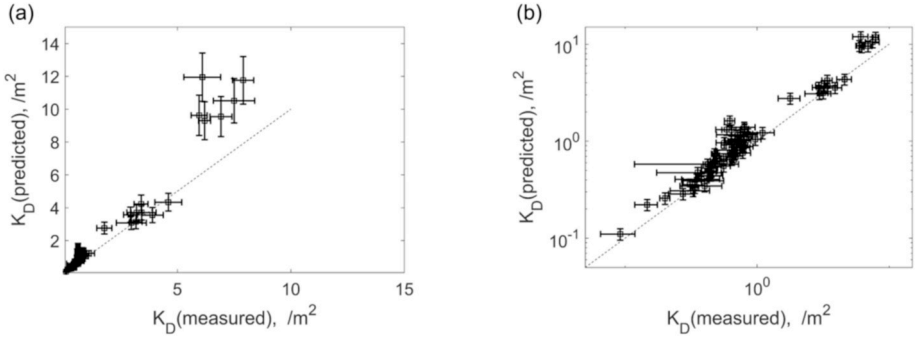


**Fig. 7.** Wave decay coefficient predicted from eqns. (18) and (19), $K_D$ (predicted), versus the measured decay coefficient, $K_D$ (measured). The dashed line denotes 1:1 agreement. Uncertainty in the measured $K_D$ (horizontal bars) came from fitting the amplitude decay along the meadow (see Methods). The uncertainty in the predicted $K_D$ (vertical bars) predominantly reflects the uncertainty in $l_r$.

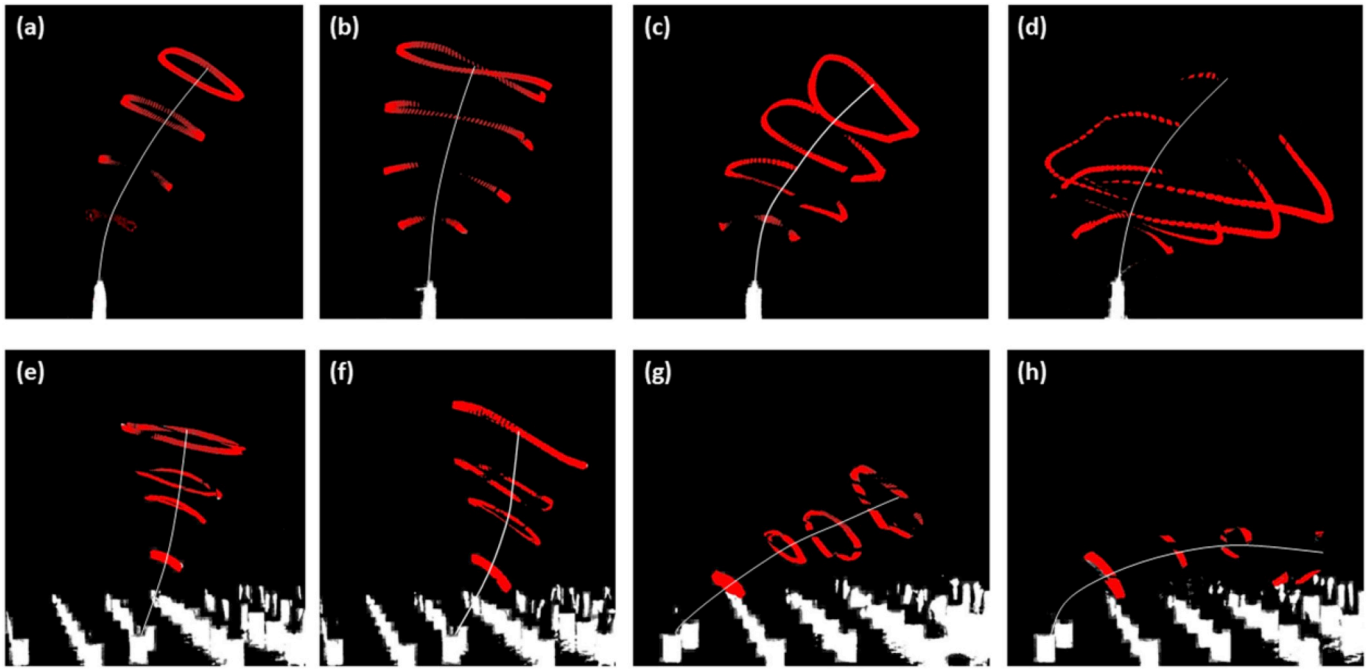


**Fig. 8.** Comparison of blade motion for a single, isolated blade attached to a stem to the motion of a blade within a meadow. Red dots trace the blade motion at different positions along the blade and over the wave cycle. The thin white line indicates the wave-cycle-average blade position. Wave period $T = 2$ s. From left to right across each row wave amplitude increased from 1.0 cm to 3.3 cm; wave orbital velocity increased from 6.5 cm/s to 13.5 cm/s; and $Ca_w$ increased from 1100 to 4800. For blades within a meadow, some parts of the blade were not visible due to sheltering from surrounding blades. The camera and the marked blade were located at mid-length of the meadow. The meadow covered the whole flume width, such that there was no open space near the sidewalls. Lateral current was not observed next to the wall. (For interpretation of the references to color in this figure legend, the reader is referred to the Web version of this article.)

$K_D(predicted) = (0.53 \pm 0.04)K_D(measured)$. This demonstrated that the inclusion of the rigid segment of the plant was necessary for good prediction.

### 3.3. Comparison of blade motion in isolation and within a meadow

At the smallest wave condition, the blade movement in the meadow (8e) matched the blade movement of the isolated blade (8a). In contrast, at the largest wave condition, the blade in the meadow was nearly horizontal (8h), significantly more pronated than the isolated blade at the same wave condition (8d). Further, for the isolated blades, the wave-cycle-average pronation (white line in Fig. 8 a, b, c, d) was similar for all wave conditions. In contrast, the wave-cycle-average pronation for the blades in a meadow (Fig. 8 e, f, g, h) increased as the wave amplitude increased. Moreover, for the blade in the meadow, the range of motion was reduced when the blade was significantly pronated. Specifically, the range of motion at the blade tip shown in Fig. 8(d) (isolated blade) was comparable to the blade length; however, the range of motion at the blade tip shown in Fig. 8(h) (blade in meadow) was only 25% of the blade length. The greater pronation of a blade within a meadow may be due to the wave-induced time-mean current generated in the meadow in the direction of wave propagation (Luhar et al. 2010, 2013; Abdolahpour et al., 2017). The current caused a mean blade pronation that did not exist for an isolated blade. The measured wave-induced current within the meadow was $U = 0.5$, 1.0, 1.2 and 1.6 cm/s, for (8e) to (8h), respectively. The significant difference in mean pronation might call into question the application of the scaling laws developed for individual blades (eqn. (17)) for prediction in a meadow. However, the good agreement between predicted and measured $K_D$ suggested that the impact of mean pronation on the wave decay was not significant. This can be explained by the fact that the upper part of the blade, where most of the mean deflection was observed, did not contribute significantly to the drag, both because the upper part of the blade moves passively with the wave (as discussed below eqn. (17), and in Luhar and Nepf 2016, and in Mullarney and Henderson 2010), and because the skin friction associated with horizontal component of the blade is negligible compared to the form drag imparted by the vertical component of the blade (e.g. eqn. (15) in Luhar and Nepf, 2011). Further, for the blades shown in Fig. 8(d) and h, $Ca_w L = 4840$, for which eqn. (17) predicted $\frac{l_e}{l} = 0.11$. Therefore, for these cases the effective blade length, which represents the near-bed blade length providing the drag, was well below the region in which the blade motion differed significantly between an isolated blade and a blade within a meadow, explaining why the visually different blade motion near the blade tip did not significantly impact the drag imparted by the blade or the wave decay.

## 4. Discussion

### 4.1. Comparison of random and regular stem arrangements

The present study used a meadow with a staggered arrangement of plants (Fig. 1). Luhar et al. (2017) made similar wave decay measurements using a meadow with a random arrangement of plants. Fig. 9 compares the measured $K_D$ for random and staggered arrays across the same range of meadow density and at the same range of $Ca_w L = 5100$ to 6500. The wave decay for random and staggered configurations agreed within uncertainty, indicating that plant configuration did not play a significant role in wave damping. Therefore, the model here should apply for any arrangement of shoots. The fact that the wave decay was not sensitive to shoot arrangement was consistent with force measurements made by Fonseca et al. (2007) on individual *Zostera marina* shoots within a meadow. Fonseca et al. (2007) reported that the difference in the mean force measured on individual shoots in a regular row arrangement versus a random arrangement was less than 7% (Table 10 in Fonseca et al., 2007). One might expect that aligned shoots would reduce the drag force on aligned neighbors, as has been observed in uni-directional current (e.g. Maza et al., 2017). The lack of

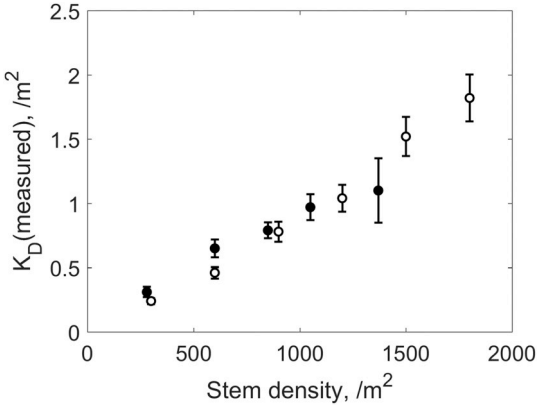


**Fig. 9.** Comparison of wave decay coefficient, $K_D$, measured over meadows with a regular staggered arrangement of shoots (black circles, present student) and a random arrangement of shoots (white circles, cases D1, D2, D3, D4, D5 and D6 in Luhar et al., 2017). For all cases $Ca_w L = 5100$ to 6500.

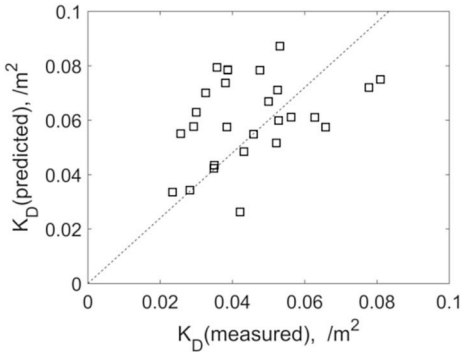


**Fig. 10.** Wave decay coefficient calculated from eqns. (18) and (19) versus the measured value reported in Fig. 5(b) in Manca et al. (2012), for which the error bars were not included. Dotted line denotes the linear-fit (i.e. $K_D(predicted) = 1.2K_D(measured)$).

arrangement dependence can be explained by the short wave conditions considered ($\leq 2.6$ s in both the present study and in Fonseca et al., 2007), for which there is little spatial variation in wave velocity. This was demonstrated in Fig. 2 of Zhang et al. (2018), which shows lateral and longitudinal transects measured in a similar model meadow. Specifically, the wave rms velocity varied by less than 5% along both transects, i.e. had little dependence on proximity to a shoot. The lack of spatial dependence in wave velocity was attributed to the small ratio of wave excursion to stem spacing. Similar behavior would not be expected for longer waves, or specifically when the wave excursion becomes very large compared to stem spacing, because at this limit the impact of the meadow on the flow approaches the behavior of an unidirectional current (Lowe et al., 2005). In unidirectional flow, aligned arrangements reduce the drag on downstream plants, because the velocity is reduced within the wakes of plants. For example, Fig. 10 in Maza et al. (2017) shows that drag force decreased with increasing distance from the leading edge of a model mangrove forest with aligned tree rows, because the downstream trees were located in the wakes of upstream trees. Similarly, Fonseca et al. (2007) found that under unidirectional flow, drag forces on individual plants within a meadow were lower in meadows with a row arrangement, compared to random arrangements.

Fig. 9 also confirmed that for the range of stem density considered in this study sheltering between blades was not important. Equation (18) indicates that $K_D$ should increase linearly with frontal area, $a_v = n_v b$. If sheltering between blades was significant, this linear dependence would be not be observed in the measured $K_D$, because sheltering decreases the frontal area felt by the flow, relative to $a_v$. Fig. 9 shows that the measured $K_D$ increased linearly with stem density, which, since there were a constant number of blades per stem, also indicated that $K_D$ increased linearly with $a_v = n_v b$. This confirmed that sheltering between blades was not important to wave decay for the stem densities considered in this study.

### 4.2. Comparison with wave decay measured in a different study

Manca et al. (2012) studied wave decay over a full-scale model of *Posidonia oceanica*. Each model plant consisted of four PVC blades inserted into a 10-cm rigid tube (Fig. 3 in Stratigaki et al., 2011). The rigid tube was partially buried, with an exposed length of $l_{stem} = 6$ cm (based on Fig. 3(b) in Stratigaki, 2011). The PVC blades had width $b = 1.2$ cm and thickness $t = 1$ mm. The tube diameter was not reported, so we assumed it was equal to the blade width, $d = 1.2$ cm. Each plant included two 55 cm-long blades and two 35 cm-long blades. For simplicity, we used the average length, $l_b = 45$ cm. Wave properties were given in Table 2 in Manca et al. (2012), including stem density, water depth, wave period, wavenumber and wave height, $H_0$. Over the range of $KC$ (140–450), the drag coefficient for the blades was $C_D = \max(10KC^{-1/3}, 1.95) = 1.95$. The drag coefficient of the tube stem was $C_{D,stem} = 1.2$ (Fig. 11 in Keulegan and Carpenter, 1958). Thus, the effective stem length $l_{stem,e} = l_{stem}\frac{C_{D,stem}d}{C_D 4b} = 0.9$ cm. Because the blades were not pinned within the tubes, we assume that the blade moved freely above the tube, so that $l_r = l_{stem,e} = 0.9$ cm. The reduction of in-canopy wave velocity relative to linear theory, $\alpha$, ranged from 0.51 to 0.89. Finally, the measured decay coefficient was given as $K_i/H_o$, with $K_i$ reported in Fig. 5(b) in Manca et al. (2012). Fig. 10 compares the predicted $K_D$ (eqn. (18) and (19)) with the measured $K_D$. A linear-fit of $K_D(predicted)$ versus $K_D(measured)$ yielded a slope of $1.2 \pm 0.6$ (95% CI), indicating a reasonable good agreement between the prediction and measurement.

### 4.3. Comparison with wave decay measured in the field

Infantes et al. (2012) measured wave decay in the field over a *Posidonia oceanica* meadow for waves with periods $T = 4 - 10$ s. Wave height was measured at four moorings across a depth gradient of 6.5 m to 16.5 m. The reported shoot length was $l_s = 0.8 \pm 0.1$ m (mean $\pm$ SE). The surface area per shoot was reported as $A_s = 211 \pm 23$ cm$^2$ (mean $\pm$ SE), and the shoot density was $n_s = 615 \pm 34$ m$^{-2}$ (mean $\pm$ SE). The frontal area per bed area was therefore $A_s n_s = 13 \pm 2$, which translated to $a_v = A_s n_s / l = 16 \pm 3$ m$^{-1}$ for an erect plant (no reconfiguration), as used in eqn. (18). *Posidonia* blades have a thickness between 0.2 and 0.5 mm (Table 1 and Marbà, 1996). We

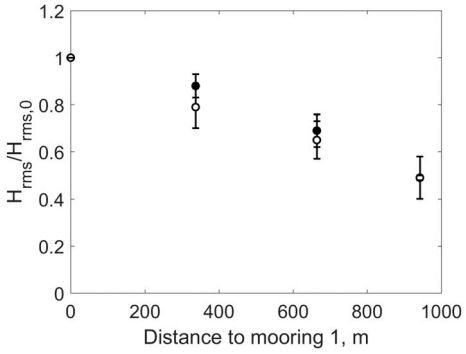


**Fig. 11.** Normalized root mean squared wave height, $H_{rms}/H_{rms,0}$. White circles denote the measured values, which represent the average wave height between 18:00h and 20:00h in Fig. 4 in Infantes et al. (2012). Black circles denote the predicted value using eqn. (20), with error bars denoting the contribution from uncertainty in the reported blade thickness, blade length, and frontal area.

assumed an average thickness of 0.35 mm. The sheath length of *Posidonia oceanica*, reported in Pergent and Pergent-Martini (1991) and Pergent et al. (1994), is 10% of the shoot length. Based on this we assumed $l_r = 0.1\, l_s$, and $l_b = 0.9\, l_s$. From Fig. 3 in Infantes et al. (2012), the rms wave velocity ranged from 0.02 to 0.18 m/s, so that $L = 2 - 47$. Based on Folkard (2005), the blade modulus of elasticity was assumed to be 0.47 GPa. The parameter $(Ca_w L)_b$ was estimated using the near-bottom, orbital velocity plotted in Fig. 3 in Infantes et al. (2012), from which the effective meadow height, $l_{m,e}$, was estimated at each mooring station using eqn. (19). For blade width $b = 9$ mm (suggested in Luhar et al. (2013)), $KC$ was 50 to 190, with an average $KC = 120$, yielding $C_D = 10KC^{-1/3} = 2.0$. Infantes et al. (2012) concluded that the impact of shoaling was negligible compared to the wave dissipation by the meadow (see Fig. 4 in Infantes et al. (2012)), so that we assumed the observed change in wave height could be attributed solely to vegetation drag. To mimic the methodology that might be applied in the field or within a numerical model, we predicted the decay of wave height along the mooring trajectory using a step size of $\Delta x = 1m$. Starting from the measured wave height at the first mooring ($H_{rms0}$), the wave height at each spatial step ($H_{rmsi}$) was estimated as

$$\frac{H_{rmsi+1}}{H_{rmsi}} = \frac{1}{1 + K_{Di} H_{rmsi} \Delta x} \tag{20}$$

with $K_{Di}$ the wave decay coefficient predicted at the $i$th spatial position. We assumed the water depth and wave orbital velocity changed linearly between the moorings. The measured wave heights were extracted from Fig. 4 in Infantes et al. (2012), with uncertainty estimated by averaging subplots from different times within the same storm event. The predicted wave height agreed with the measured wave heights within uncertainty.

## 5. Summary

This paper described and validated a new model to predict the dissipation of wave energy over a submerged meadow of flexible plants. Because part of the plant moves passively with the wave, the vegetation drag and thus wave decay are diminished relative to that for a fully rigid blade of the same geometry. The impact of reconfiguration on wave decay can be characterized using an effective blade length, $l_e$, which represents the length of a rigid blade that generates the same drag as the flexible blade of length $l$. Measurements of drag on individual blades were used to validate a blade scaling law, $l_e/l = 0.94(Ca_w L)^{-0.25}$. Model seagrass shoots were constructed with six blades attached to a cylindrical stem, representing the sheath of a real seagrass shoot. To reflect that the individual shoots consisted of both rigid and freely moving lengths, the total shoot height was broken into rigid ($l_r$) and freely moving ($l_b$) segments. The freely moving segment was assumed to behave like an isolated blade, and its effective length ($l_{b,e}$) was determined from the blade scaling law. The wave decay over a meadow of shoots was then be predicted using the effective meadow height, $l_{e,m} = l_{b,e} + l_r$. The predicted wave decay agreed with the measured wave decay to within an average of 16%. The model also produced good predictions for a different laboratory study and a field study. Finally, wave decay was similar over meadows with regular and random arrangements of shoots, which was explained by the lack of spatial variation in wave orbital velocity for conditions with orbital excursions less than or comparable to the shoot spacing.

## Acknowledgement

This material is based upon work supported by the National Science Foundation under grant EAR 1659923. Any opinions, findings, and conclusions or recommendations expressed in this material are those of the author(s) and do not necessarily reflect the views of the National Science Foundation. Data may be obtained from Jiarui Lei (email: garylei@mit.edu).

## Appendix A. Supplementary data

Supplementary data to this article can be found online at https://doi.org/10.1016/j.coastaleng.2019.01.008.

## References

Abdelrhman, M., 2007. Modeling coupling between eelgrass Zostera marina and water flow. Mar. Ecol. Prog. Ser. 338, 81–96. https://doi.org/10.3354/meps338081.
Abdolahpour, M., Hambleton, M., Ghisalberti, M., 2017. The wave-driven current in coastal canopies. JGR-Oceans 122, 3660–3674. https://doi.org/10.1002/2016JC012446.
Arkema, K., Griffin, R., Maldonado, S., Silver, J., Suckale, J., Guerry, A., 2017. Linking social, ecological, and physical science to advance natural and nature-based protection for coastal communities. Ann. N. Y. Acad. Sci. https://doi.org/10.1111/nyas.13322.
Barbier, E., Hacker, S., Kennedy, C., Koch, E., Stier, A., Silliman, B., 2011. The value of estuarine and coastal ecosystem services. Ecol. Monogr. 81 (2), 169–193. https://doi.org/10.1890/10-1510.1.
Bradley, K., Houser, C., 2009. Relative velocity of seagrass blades: implications for wave attenuation in low-energy environments. JGR Earth Surface 114 (F1). https://doi.org/10.1029/2007JF000951.
Costanza, R., d'Arge, R., De Groot, R., Farber, S., Grasso, M., Hannon, B., Limburg, K., Naeem, S., O'neill, R.V., Paruelo, J., Raskin, R.G., 1997. The value of the world's ecosystem services and natural capital. Nature 387 (6630), 253–260. https://doi.org/10.1038/387253a0.
Dalrymple, R., Kirby, J., Hwang, P., 1984. Wave diffraction due to areas of energy dissipation. J. Waterw. Port, Coast. Ocean Eng. 110 (1), 67–79. https://doi.org/10.1061/(ASCE)0733-950X(1984)110:1(67).
Döbken, J.W., 2015. Modeling the Interaction of Wave Hydrodynamics with Flexible Aquatic Vegetation. Master thesis. Deltares. TU Delft.
Fonseca, M., Koehl, M., Kopp, B., 2007. Biomechanical factors contributing to self-organization in seagrass landscapes. J. Exp. Mar. Bio. Ecol. 340 (2), 227–246. https://doi.org/10.1016/j.jembe.2006.09.015.
Folkard, A., 2005. Hydrodynamics of model *Posidonia oceanica* patches in shallow water. Limnol. Oceanogr. 50 (5), 1592–1600. https://doi.org/10.4319/lo.2005.50.5.1592.
Fourqurean, J., Duarte, C., Kennedy, H., Marba, N., Holmer Apostolaki, E.T, M., Kendrick, G.A., Krause-Jensen, D., McGlathery, K.J., Serrano, O., 2012. Seagrass ecosystems as a globally significant carbon stock. Nat. Geosci. 5 (7), 505. https://doi.org/10.1038/ngeo1477.
Gacia, E., Duarte, C., 2001. Sediment retention by a Mediterranean *Posidonia oceanica* meadow: the balance between deposition and resuspension. Estuar. Coast Shelf Sci. 52 (4), 505–514. https://doi.org/10.1006/ecss.2000.0753.
Ghisalberti, M., Nepf, H., 2002. Mixing layers and coherent structures in vegetated aquatic flow. JGR-Oceans 107 (C2). https://doi.org/10.1029/2001JC000871.
Gijon Mancheno, A., 2016. Interaction between Wave Hydrodynamics and Flexible Vegetation. Master's thesis. TU Delft, Delft, Netherlands.
Goda, Y., Suzuki, Y., 1977. Estimation of incident and reflected waves in random wave experiments. Coast. Eng. 1976, 828–845. https://doi.org/10.1061/9780872620834.048.
Greiner, J., McGlathery, K., Gunnell, J., McKee, B., 2013. Seagrass restoration enhances "blue carbon" sequestration in coastal waters. PLoS One 8 (8), e72469. https://doi.org/10.1371/journal.pone.0072469.
Gruber, R.K., Kemp, W.M., 2010. Feedback effects in a coastal canopy-forming submersed plant bed. Limnol. Oceanogr. 55 (6), 2285–2298. https://doi.org/10.4319/lo.2010.55.6.2285.
Houser, C., Trimble, S., Morales, B., 2015. Influence of blade flexibility on the drag coefficient of aquatic vegetation. Estuar. Coasts 38 (2), 569–577. https://doi.org/10.1007/s12237-014-9840-3.
Hunt, J.N., 1964. The viscous damping of gravity waves in shallow water. La Houille Blanche 6, 685–691.
Infantes, E., Orfila, A., Terrados, J., Luhar, M., Simarro, G., Nepf, H., 2012. Effect of a seagrass (*Posidonia oceanica*) meadow on wave propagation. Mar. Ecol. Prog. Ser. 456, 63–72. https://doi.org/10.3354/meps09754.
Keulegan, G., Carpenter, L.H., 1958. Forces on cylinder and plates in an oscillating fluid. J. Res. Natl. Bur. Stand. 60 (5), 423–440. https://doi.org/10.6028/jres.060.043.
Losada, I.J., Maza, M., Lara, J.L., 2016. A new formulation for vegetation-induced damping under combined waves and currents. Coast. Eng. 107, 1–13. https://doi.org/10.1016/j.coastaleng.2015.09.011.
Lowe, R.J., Koseff, J.R., Monismith, S.G., 2005. Oscillatory flow through submerged canopies: 1. Velocity structure. J. Geophys. Res.: Oceans 110 (C10). https://doi.org/10.1029/2004JC002788.
Luhar, M., Coutu, S., Infantes, E., Fox, S., Nepf, H., 2010. Wave induced velocities inside a model seagrass bed. JGR-Oceans 115, C12005. https://doi.org/10.1029/2010JC006345.
Luhar, M., Nepf, H., 2011. Flow induced reconfiguration of buoyant and flexible aquatic vegetation. Limnol. Oceanogr. 56 (6), 2003–2017. https://doi.org/10.4319/lo.2011.56.6.2003.
Luhar, M., Infantes, E., Orfila, A., Terrados, J., Nepf, H., 2013. Field observations of wave-induced streaming through a submerged seagrass (*Posidonia oceanica*) meadow. JGR-Oceans 118 (4), 1955–1968. https://doi.org/10.1002/jgrc.20162.
Luhar, M., Nepf, H., 2016. Wave-induced dynamics of flexible blades. J. Fluid Struct. 61, 20–41. https://doi.org/10.1016/j.jfluidstructs.2015.11.007.
Luhar, M., Infantes, E., Nepf, H., 2017. Seagrass blade motion under waves and its impact

on wave decay. JGR-Oceans 122. https://doi.org/10.1002/2017JC012731.
Manca, E., Cáceres, I., Alsina, J., Stratigaki, V., Townend, I., Amos, C., 2012. Wave energy and wave-induced flow reduction by full-scale model *Posidonia oceanica* seagrass. Cont. Shelf Res. 50, 100–116. https://doi.org/10.1016/j.csr.2012.10.008.
Marbà, N., Duarte, C.M., Cebrián, J., Gallegos, M.E., Olesen, B., Sand-Jensen, K., 1996. Growth and population dynamics of Posidonia oceanica on the Spanish Mediterranean coast: elucidating seagrass decline. Mar. Ecol. Prog. Ser 137, 203–213.
Maza, M., Lara, J., Losada, I., 2013. A coupled model of submerged vegetation under oscillatory flow using Navier–Stokes equations. Coast. Eng. 80, 16–34. https://doi.org/10.1016/j.coastaleng.2013.04.009.
Maza, M., Adler, K., Ramos, D., Garcia, A.M., Nepf, H., 2017. Velocity and drag evolution from the leading edge of a model mangrove forest. J. Geophys. Res. Ocean. 122 (11), 9144–9159. https://doi.org/10.1002/2017JC012945.
McKone, K.L., 2009. *Light available to the seagrass zostera marina when exposed to currents and waves* (Order No. 1465547). Available from: ProQuest Dissertations & Theses Global. (304923463). Retrieved from. https://search.proquest.com/docview/304923463?accountid=12492.
Mendez, F., Losada, I., Losada, M., 1999. Hydrodynamics induced by wind waves in a vegetation field. JGR-Oceans 104 (C8), 18383–18396. https://doi.org/10.1029/1999JC900119.
Mendez, F., Losada, I., 2004. An empirical model to estimate the propagation of random breaking and nonbreaking waves over vegetation fields. Coast. Eng. 51 (2), 103–118. https://doi.org/10.1016/j.coastaleng.2003.11.003.
Moore, K., 2004. Influence of seagrasses on water quality in shallow regions of the lower Chesapeake Bay. J. Coast Res. 162–178. https://doi.org/10.2112/SI45-162.1.
Mullarney, J., Henderson, S., 2010. Wave-forced motion of submerged single-stem vegetation. JGR- Oceans 115 (C12). https://doi.org/10.1029/2010JC006448.
Pergent, G., Pergent-Martini, C., 1991. Leaf renewal cycle and primary production of Posidonia oceanica in the bay of Lacco Ameno (Ischia, Italy) using lepidochronological analysis. Aquat. Bot. 42 (1), 49–66. https://doi.org/10.1016/0304-3770(91)90105-E.
Pergent, G., Romero, J., Pergent-Martini, C., Mateo, M.A., Boudouresque, C.F., 1994. Primary production, stocks and fluxes in the Mediterranean seagrass Posidonia oceanica. Mar. Ecol. Prog. Ser. 139–146. https://doi.org/10.3354/meps106139.
Sarpkaya, T., O'Keefe, J., 1996. Oscillating flow about two and three-dimensional bilge keels. Trans. ASME-J. Offshore Mech. Arctic. Eng. 118 (1), 1–5. https://doi.org/10.1115/1.2828796.
Stratigaki, V., Manca, E., Prinos, P., Losada, I., Lara, J., Sclavo, M., Sánchez-Arcilla, A., 2011. Large-scale experiments on wave propagation over *Posidonia oceanica*. J. Hydraul. Res. 49 (Suppl. 1), 31–43. https://doi.org/10.1080/00221686.2011.583388.
Sutton-Grier, A., Wowk, K., Bamford, H., 2015. Future of our coasts: the potential for natural and hybrid infrastructure to enhance the resilience of our coastal communities, economies and ecosystems. Environ. Sci. Policy 51, 137–148. https://doi.org/10.1016/j.envsci.2015.04.006.
Wang, J., Pang, Y., Li, Y., Huang, Y., Luo, J., 2015. Experimental study of wind-induced sediment suspension and nutrient release in Meiliang Bay of Lake Taihu, China. Environ. Sci. Pollut. Control Ser. 22 (14), 10471–10479. https://doi.org/10.1007/s11356-015-4247-7.
Waycott, M., Longstaff, B., Mellors, J., 2005. Seagrass population dynamics and water quality in the Great Barrier Reef region: a review and future research directions. Mar. Pollut. Bull. 51 (1), 343–350. https://doi.org/10.1016/j.marpolbul.2005.01.017.
Weitzman, J.S., Aveni-Deforge, K., Koseff, J.R., Thomas, F.I.M., 2013. Uptake of dissolved inorganic nitrogen by shallow seagrass communities exposed to wave-driven unsteady flow. Mar. Ecol. Prog. Ser. 475, 65–83. https://doi.org/10.3354/meps09965.
Zeller, R., Weitzman, J., Abbett, M., Fringer, F. Zarama O., Koseff, J., 2014. Improved parameterization of seagrass blade dynamics and wave attenuation based on numerical and laboratory experiments. Limnol. Oceanogr. 59 (1), 251–266. https://doi.org/10.4319/lo.2014.59.1.0251.
Zhang, Y., Tang, C., Nepf, H., 2018. Turbulent kinetic energy in submerged model canopies under oscillatory flow. Water Res. Res. 54 (3), 1734–1750. https://doi.org/10.1002/2017WR021732.